Broadband 2 μm fluorescence and energy transfer evaluation in Ho3+/Er3+ codoped germanosilicate glass

ARTICLE *in* JOURNAL OF QUANTITATIVE SPECTROSCOPY AND RADIATIVE TRANSFER · AUGUST 2015

Impact Factor: 2.65 · DOI: 10.1016/j.jqsrt.2015.03.035

7 AUTHORS, INCLUDING:

Ying Tian

China Jiliang University

89 PUBLICATIONS **762** CITATIONS

SEE PROFILE

Xufeng Jing

China Jiliang University

45 PUBLICATIONS **176** CITATIONS

SEE PROFILE

Junjie Zhang

China Jiliang University

207 PUBLICATIONS **2,500** CITATIONS

SEE PROFILE

Journal of Quantitative Spectroscopy & Radiative Transfer 161 (2015) 95–104

Contents lists available at ScienceDirect

Journal of Quantitative Spectroscopy & Radiative Transfer

journal homepage: www.elsevier.com/locate/jqsrt

Broadband 2 μm fluorescence and energy transfer evaluation in Ho^{3+}/Er^{3+} codoped germanosilicate glass

Tao Wei [a], Cong Tian [b], Muzhi Cai [a], Ying Tian [a,*], Xufeng Jing [c], Junjie Zhang [a], Shiqing Xu [a,*]

[a] College of Materials Science and Engineering, China Jiliang University, Hangzhou 310018, PR China
[b] College of Mathematics, Physics and Information Engineering, Zhejiang Normal University, Jinhua, Zhejiang 321004, PR China
[c] Institute of Optoelectronic Technology, China Jiliang University, Hangzhou 310018, PR China

ARTICLE INFO

Article history:
Received 15 December 2014
Received in revised form
23 March 2015
Accepted 24 March 2015
Available online 11 April 2015

Keywords:
Ho^{3+}/Er^{3+} codoped germanosilicate glass
2 μm Fluorescence
Gain bandwidth
Energy transfer
Rate equation

ABSTRACT

This work reports the broadband 2 μm emission from Ho^{3+}/Er^{3+} codoped germanosilicate glasses. Spectral components of the 2 μm emission band were analyzed and an equivalent model of four-level system was proposed to describe the 2 μm emission band. The results suggested that Ho^{3+}/Er^{3+} codoped germanosilicate glass has high effective emission bandwidth (172 nm), large emission cross section (5.18×10^{-21} cm^2) and gain bandwidth (891×10^{-28} cm^3), which is a promising candidate for 2 μm laser and amplifier. In addition, energy transfer mechanism between Ho^{3+} and Er^{3+} ions was investigated based on the measured fluorescence spectra and decay curves of Er^{3+}:$^4I_{11/2}$ and $^4I_{13/2}$ levels. Energy transfer efficiency and microscopic parameters were calculated to evaluate the 2 μm fluorescence. Moreover, a rate equation model between Ho^{3+} and Er^{3+} ions was developed to elucidate 2 μm fluorescence behaviors. This work might provide useful guide to investigate fluorescence behavior and energy transfer mechanism of rare earth ions.

1. Introduction

In recent years, considerable efforts have been devoted to obtain efficient and powerful mid-infrared lasers and amplifiers operating in the eye-safe 2 μm wavelength region. This is due to their potential applications, including coherent laser radar systems, laser imaging, biomedical systems, remote chemical sensing and pump sources for mid-infrared lasers as well as optical communication systems [1–3].

So far, 2 μm laser is mainly achieved from Tm^{3+} or Ho^{3+} ions. In 2009, single- frequency ~2 μm laser was demonstrated in Tm-doped silicate glass fiber with laser linewidth less than 3 kHz using a single-mode Er-doped fiber laser at 1575 nm as a core-pump source [4]. In 2013, a direct diode-pumped monolithic thulium doped fiber laser was reported [5]. It offered more than 250 nm continuous total tuning range and a 3 dB power flatness of 200 nm [5]. In addition, a multiple-watt Tm^{3+}/Ho^{3+} codoped aluminosilicate glass fiber laser operating in narrowband (<0.5 nm) and tuned across a range exceeding 280 nm was presented in 2010 [3]. Its maximum slope efficiency and average output power were 25% and 6.8 W at 2.04 μm. In 2012, a single-frequency gain-switched Ho-doped silicate fiber laser was also achieved with output wavelength at 2.05 μm [6].

Compared with Tm^{3+}, the emission cross section of Ho^{3+} ion is much larger, which makes Ho^{3+} ions more suitable for high efficient laser operation [7]. Unfortunately,

* Corresponding authors. Tel.: +86 571 8683 5781; fax: +86 571 2888 9527.
E-mail addresses: tianyingcjlu@163.com (Y. Tian), shiqingxu75@163.com (S. Xu).

http://dx.doi.org/10.1016/j.jqsrt.2015.03.035
0022-4073/

Ho^{3+} can not be pumped directly by readily available commercial high-power 808 nm or 980 nm laser diodes owing to the lack of an appropriate absorption band [1]. Hence, Yb^{3+}, Tm^{3+}, Nd^{3+} and Er^{3+} with a strong absorption band near 808 nm or 980 nm wavelengths have been utilized as the sensitizer to solve this problem [1,8–10]. So far, Ho^{3+}/Yb^{3+} codoped [8,11,12], Ho^{3+}/Tm^{3+} codoped [13–15], and Ho^{3+}/Nd^{3+} codoped [1,16] glasses have been investigated by researchers. However, to our knowledge, Er^{3+} sensitized Ho^{3+} doped glasses are less reported for 2 μm radiations but some investigations on upconversion and energy transfer process [10,17].

On the other hand, suitable glass host is as important as the luminescent ion. Recent decades have witnessed the great development on various glasses such as fluorophosphates [12,18], tellurite [19,20], germanate [7,21] and bismuthate glass [22]. In 2009, Wang et al. reported 2 μm fluorescence properties in Ho^{3+} doped fluorophosphate glasses sensitized with Er^{3+} and Tm^{3+} under 800 nm pumping [23]. Energy transfer mechanism of Ho^{3+}-Er^{3+}-Tm^{3+} ions was discussed in detail [23]. Simultaneously, Gao et al. investigated the 2 μm emission in Tm^{3+} and Ho^{3+} codoped TeO_2–ZnO–Bi_2O_3 glasses [24,25]. High radiative transition probabilities and large emission cross sections were obtained [24]. Besides, in 2010, Xu et al. reported Yb^{3+}/Ho^{3+} codoped germanate glass with high 2 μm emission cross section of Ho^{3+} and efficient energy transfer of $Yb^{3+} \rightarrow Ho^{3+}$ [7].

Germanosilicate glass, which combines the advantages of higher index of refractionof germanate glass and low cost together with higher thermal stability of silicate glass, is a promising candidate for 2 μm laser material [26]. In our previous work, germanosilicate glass has been investigated for 1.53 μm optical amplifier and results indicate that broadband 1.53 μm emission can be achieved from Er^{3+} doped germanosilicate glass [26,27]. Therefore, it is expected that broadband 2 μm radiation can also be obtained from Ho^{3+} activated germanosilicate glass for laser and amplifier.

In this work, Ho^{3+}/Er^{3+} codoped germanosilicate glasses were prepared for 2 μm emissions. Spectroscopic properties of Ho^{3+} and energy transfer mechanism between Er^{3+} and Ho^{3+} ions were discussed in detail. Energy transfer efficiency and microscopic parameters were calculated based on absorption spectra and lifetime measurements. Moreover, a rate equation model was developed to elucidate 2 μm emission behaviors.

2. Experimental

Host glasses possessing the compositions of $30SiO_2$–$30GeO_2$–8CaO–$12Li_2O$–$5Nb_2O_5$–15BaO (in mol%) were prepared by melting-quenching technique with an analytic reagent as raw materials. External co-doping of 1 mol% Er_2O_3 (99.99%) and x mol% Ho_2O_3 (99.99%) (x=0.25; 0.5; 0.75; 1) were carried out, which is named as SGEH-x. In addition, Ho^{3+} and Er^{3+} singly doped samples were also prepared for the comparisons and denoted as SGH and SGE, respectively. Raw materials (20 g) were mixed homogeneously and melted in a platinum crucible in a SiC-resistance electric furnace at 1450 °C for 45 min. Then the melts were quenched on preheated stainless steel plate and annealed at 10 °C below the glass transition temperature (580–590 °C) for 4 h before they were cooled to room temperature. Finally, the annealed samples were fabricated and optically polished to the size of 10 mm × 10 mm × 1.5 mm for the optical property measurement.

The densities and refractive indexes of the prepared glasses were tested according to the Archimedes principle using distilled water as the immersion medium and the prism minimum deviation method, respectively. Absorption spectra were determined by means of a Perkin Elmer Lambda 900UV–vis–NIR spectrophotometer in the range of 300–2200 nm with the resolution of 1 nm. Fluorescence spectra (900–2800 nm) were measured with a computer-controlled Triax 320 type spectrometer upon excitation by 808 nm laser diode with the maximum power of 1 W. Fluorescence lifetimes of $^4I_{11/2}$ level (975 nm) and $^4I_{13/2}$ level (1.53 μm) were recorded with light pulses of the 808 nm LD and HP546800B 100-MHz oscilloscope. All the measurements were carried out at room temperature.

3. Results

3.1. Absorption spectra

Fig. 1 shows the absorption spectra of Er^{3+}, Ho^{3+} singly doped and Ho^{3+}/Er^{3+} codoped germanosilicate glasses in the spectral region of 300–2200 nm. The absorption spectra are characterized by absorption bands of Er^{3+} (from the ground level of $^4I_{15/2}$ to the excited levels of $^4I_{13/2}$, $^4I_{11/2}$, $^4I_{9/2}$, $^4F_{9/2}$, $^4S_{3/2}$, $^2H_{11/2}$ and $^4F_{7/2}$) and Ho^{3+} (from the ground state ($^5I_8$) to higher levels of $^5I_7$, $^5I_6$, $^5I_5$, $^5F_5$ and $^5F_4+^5S_2$, respectively). No shape change and peak position shift of Ho^{3+}/Er^{3+} absorption bands can be observed with increasing Ho^{3+} concentration as is shown in the inset of Fig. 1. For Ho^{3+} singly doped sample, no absorption bands match readily available 808 or 980 LDs. Ho^{3+}/Er^{3+} codoped samples show an absorption band of Er^{3+}: $^4I_{15/2} \rightarrow {}^4I_{9/2}$ around 808 nm, which matches commercialized 808 nm LD.

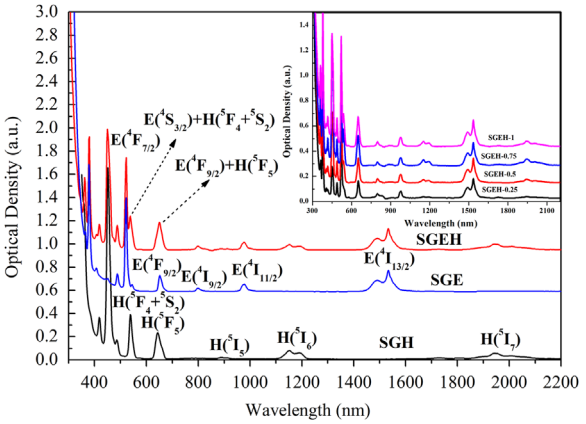

Fig. 1. Absorption spectra of Er^{3+}, Ho^{3+} singly doped and Er^{3+}/Ho^{3+} codoped germanosilicate glasses. Inset of the figure represents the peak shape and positions varied with Ho^{3+} concentrations of all prepared samples.

3.2. J–O analysis and radiative properties

In order to investigate the local environment around Ho^{3+} ions, *J–O* intensity parameters have been calculated by fitting the experimental and calculated oscillator strengths based on absorption spectrum of Ho^{3+} and *J–O* theory [28,29]. The detailed calculation procedures have been well described elsewhere [30]. The measured (f_{mea}) and calculated (f_{cal}) oscillator strengths of SGH sample and other reported glass systems were listed in Table 1. Good agreement between f_{mea} and f_{cal} can be observed, which proofed by the small root mean square deviation δ_{rms} of 1.27×10^{-6}. It is interesting that the hypersensitive transition (HST)of $^5I_8\rightarrow{}^5F_1+{}^5G_6$ possesses the highest oscillator strength. It is reported that the oscillator strength of the HST depends strongly on the glass matrixes, and is sensitive to minor changes of local environment around Ho^{3+} ions and affects the *J–O* intensity parameters [31,32]. As shown in Table 1, it can be noticed that the oscillator strengths of SHG glass are higher than those of silicate and germanate glass. This can be ascribed to the divergence of ligand field derived from various glass compositions. *J–O* parameters were obtained for further estimation of the difference of ligand field in glasses below.

Table 2 summarizes the *J–O* intensity parameters (Ω_λ, $\lambda=2,4,6$) ($\times10^{-20}$ cm^2) of Ho^{3+} ions in various glass hosts. The calculated intensity parameters of germanosilicate glass follow the trend of $\Omega_2>\Omega_4>\Omega_6$, which is consistent with those of tellurite, germanate and silicate glasses whereas it differs from those of fluoride and fluorophosphate glass as shown in Table 2. Previous studies indicated that parameter Ω_2 is indicative of the extent of covalent bonding and is strongly dependent on the local environments of Ho^{3+} ions [23]. It can be found from Table 2 that the prepared germanosilicate glass possesses higher Ω_2 value when compared with fluoride [33], fluorophosphate [33], tellurite [34] and silicate glass [23] whereas the Ω_2 value is a little lower than that of germanate glasses [35]. It is suggested that the prepared germanosilicate glass possesses higher covalency around Ho^{3+} ions than fluoride, fluorophosphate, tellurite and silicate glasses.

The radiative properties of Ho^{3+} in germanosilicate glass are evaluated via *J–O* parameters, such as radiative transition probability (A_{rad}), fluorescence branching ratios (β) and radiative lifetimes (τ_{rad}) of some transition levels. The calculated values are presented in Table 3. It is found that the A_{rad} of Ho^{3+}: $^5I_7\rightarrow{}^5I_8$ transition is 131.36 s^{-1} for the studied sample, which is larger than those of fluorophosphate (70.98 s^{-1}) [23], tellurite (104 s^{-1}) [34] and germanate glasses (69.2 s^{-1}) [15].

3.3. Analysis of fluorescence spectra at 2 μm and emission cross sections

Fig. 2 presents the fluorescence spectra of Ho^{3+}/Er^{3+} codoped germanosilicate glasses in the spectral region of 1800–2200 nm pumped at 808 nm as a function of Ho^{3+} doping concentration. Moreover, 2 μm emission intensity dependence of Ho^{3+} concentration is also plotted in the

Table 3
Radiative transition probability (A_{rad}), fluorescence branching ratios (β) and radiative lifetimes (τ_{rad}) of Ho^{3+} ions for different transitions.

Transition	Energy gap (cm^{-1})	A_{rad} (s^{-1})	β (%)	τ_{rad} (ms)
$^5I_7\rightarrow{}^5I_8$	5128	131.36	100	7.61
$^5I_6\rightarrow{}^5I_8$	8681	223.54	82.80	3.70
$^5I_6\rightarrow{}^5I_7$	3552	46.44	17.20	–
$^5I_5\rightarrow{}^5I_8$	11236	81.25	39.25	4.83
$^5I_5\rightarrow{}^5I_7$	6108	107.21	51.79	–
$^5I_5\rightarrow{}^5I_6$	2555	18.56	8.97	–

Table 1
Measured (f_{mea}) and calculated (f_{cal}) oscillator strengths of SGH sample and compared with other systems.

Absorption	λ (nm)	Oscillator strength		Silicate[9]	Germanate[15]
		$f_{mea}(\times10^{-6})$	$f_{cal}(\times10^{-6})$	$f_{mea}(\times10^{-6})$	$f_{mea}(\times10^{-6})$
$^5I_8\rightarrow{}^5I_6$	1152	0.907	1.051	0.455	0.605
$^5I_8\rightarrow{}^5F_5$	644	3.464	3.478	1.810	2.380
$^5I_8\rightarrow{}^5F_4+{}^5S_2$	538	4.838	3.435	2.577	3.017
$^5I_8\rightarrow{}^5F_1+{}^5G_6$	452	28.28	28.257	14.358	14.504
$^5I_8\rightarrow{}^5G_5$	418	2.998	4.133	1.393	2.346
δ_{rms}		1.27×10^{-6}			

Table 2
J–O intensity parameters (Ω_λ, $\lambda=2,4,6$) ($\times10^{-20}$ cm^2) of Ho^{3+} ions in various glass hosts.

Samples	Ω_2	Ω_4	Ω_6	Trend	Reference
SGH	6.02 ± 0.12	3.02 ± 0.10	1.36 ± 0.15	$\Omega_2>\Omega_4>\Omega_6$	Present work
Silicate	5.20	1.80	1.20	$\Omega_2>\Omega_4>\Omega_6$	[23]
Fluoride	1.86	1.90	1.32	$\Omega_4>\Omega_2>\Omega_6$	[33]
Fluorophosphate	3.11	3.50	1.65	$\Omega_4>\Omega_2>\Omega_6$	[33]
Tellurite	3.78	2.23	1.85	$\Omega_2>\Omega_4>\Omega_6$	[34]
Germanate	6.60	1.75	0.99	$\Omega_2>\Omega_4>\Omega_6$	[35]

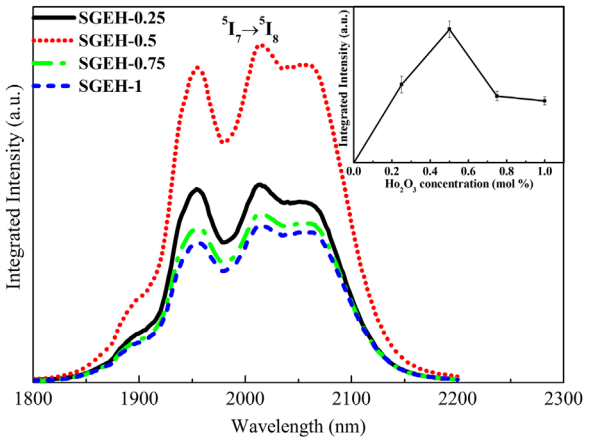

Fig. 2. Fluorescence spectra of Ho^{3+} doped germanosilicate glasses sensitized by Er^{3+} pumped at 808 nm. The inset is 2 μm emission intensity dependence of Ho^{3+} concentration.

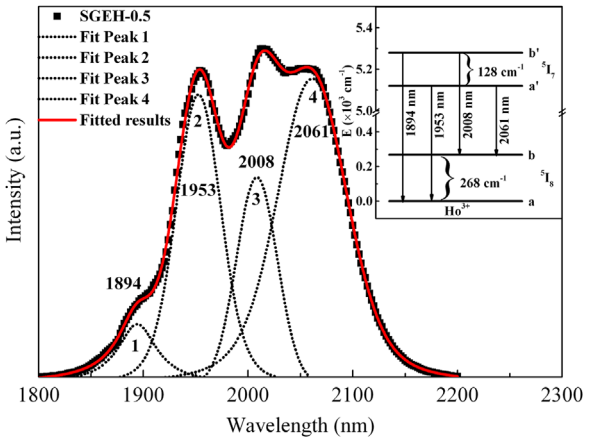

Fig. 3. Deconvolution of 2 μm emission spectra of Ho^{3+} in germanosilicate glass using Gaussian functions. The inset is an equivalent model of four-level system for describing the 2 μm fluorescence band.

inset of Fig. 2. A broad emission band near 2 μm corresponding to $^5I_7 \rightarrow {}^5I_8$ transition of Ho^{3+} can be observed. With increasing Ho^{3+} concentration, the fluorescent intensity increases firstly since the more luminescent centers of Ho^{3+} accept energy transferred from Er^{3+} ions, attains a maximum for Ho^{3+} concentration of 1 mol% and then decreases shown in Fig. 2 and inset of Fig. 2. This can be attributed to the greatly enhanced interaction between Ho^{3+} and Er^{3+} ions and the rise of concentration quenching. Thus, the optimal Ho^{3+} concentration is 1 mol% (SGEH-0.5). This will further be demonstrated by the calculations of rate equation equations.

Interestingly, the 2 μm fluorescence band shows a non-Gaussian peak shape consisting of several Stark emission bands. The Gaussian deconvolution procedure is carried out to verify the spectral components of 2 μm emission peaks and the result is displayed in Fig. 3. It can be observed that the wavelengths of four Gaussian profiles are centered at 1894 nm, 1953 nm, 2008 nm and 2061 nm. In parallel, an equivalent model of four-level system for describing the 2 μm fluorescence band is also illustrated in the inset of Fig. 3. The ground state $^5I_8$ is composed of the two Stark levels of lower a and upper b. In the same way, the $^5I_7$ level contains two Stark levels of lower a′ and upper b′. The b′ → a, a′ → a, b′ → b and a′ → b transitions correspond to peak 1, 2, 3 and 4, respectively, as presented in Fig. 3. The Stark splitting energy of $^5I_8$ level is about 268 cm^{-1}, which is larger than that of $^5I_7$ level (128 cm^{-1}) in Ho^{3+} activated germanosilicate glass. Moreover, the Gaussian peak positions have minor shifts in comparison to other reported results [13]. This indicates that the extent of the Stark splitting is closely dependent on the glass compositions.

Emission cross section is an important parameter to estimate the possibility for achieving laser action. Higher emission cross section means that better laser gain can be achieved in glasses [8,36]. Emission cross section ($\sigma_{em}(\lambda)$) at 2 μm can be calculated by Füchtbauer–Ladenburg (FL) equation [37]

$$\sigma_{em}(\lambda) = \frac{\lambda^4 A_{rad}}{8\pi c n^2} \times \frac{\lambda I(\lambda)}{\int \lambda I(\lambda) d\lambda} \quad (1)$$

where λ is the emission wavelength, A_{rad} is the spontaneous radiative transition probability of Ho^{3+}: $^5I_7 \rightarrow {}^5I_8$ transition, c is the velocity of light in vacuum, n is the refractive index of glass host, $I(\lambda)$ is the 2 μm fluorescence intensity, and $\int I(\lambda) d\lambda$ is the integrated fluorescence intensity. The calculated emission cross section of Ho^{3+}: $^5I_7 \rightarrow {}^5I_8$ transition is plotted in Fig. 4. It can be obtained that the peak emission cross section at 2 μm is as high as 5.18×10^{-21} cm^2. It is larger than that of silicate glass (3.54×10^{-21} cm^2) [9], slightly lower than that of germanate glass (8.00×10^{-21} cm^2) [21], and comparable to that of germanate–tellurite glass (4.36×10^{-21} cm^2) [8]. High emission cross section makes the prepared germanosilicate glass an attractive candidate for 2 μm laser.

Besides, effective emission bandwidth ($\Delta\lambda_{eff}$) has been calculated according to the following equation [36]:

$$\Delta\lambda_{eff} = \frac{\int \sigma_{em}(\lambda)}{\sigma_{em}^{peak}} \quad (2)$$

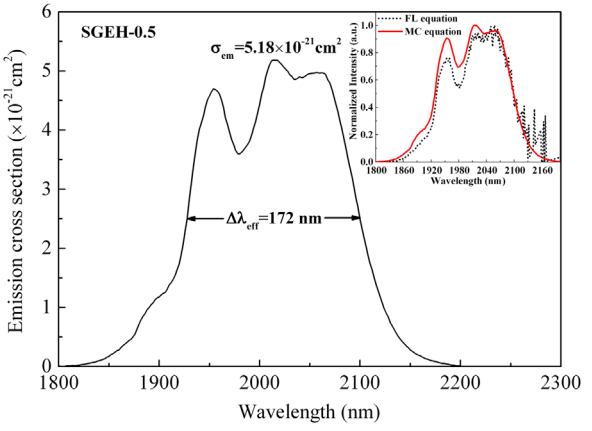

Fig. 4. Emission cross section of Ho^{3+} doped germanosilicate glass. The inset is the normalized emission cross sections at 2 μm calculated by FL equation and MC formula, respectively.

where σ_{em}^{peak} is the peak emission cross section at 2 μm. It is reasonable to select effective emission bandwidth other than the full width at half maximum because the 2 μm emission band of Ho^{3+} ions in glass is asymmetric as presented in Fig. 4. For broadband optical amplifier, it is required that effective emission bandwidth is as wide as possible to provide multiple channels for signal transmission. It is calculated from Fig. 4 that $\Delta\lambda_{eff}$ value can reach 172 nm, which is larger than those of tellurite glass (160 nm) [38], fluoride glass (118 nm) [33] and fluorophosphate glass (150 nm) [33]. The higher effective emission bandwidth can be attributed to the existence of various structural unites such as SiO_4 and GeO_4 of germanosilicate glass [39,40]. The different Ge–O and Si–O bond lengths associated with these various structural units lead to multiplicity of ion-ion field strengths. Therefore, the divergences yield a range of electro-static fields around Ho^{3+} ions in germanosilicate glasses. Thus, an inhomogeneous broadening of the fluorescent band can be achieved [38,39].

Fluorescence trapping, which induces spectral broadening, exists for Ho^{3+}:$^5I_7 \rightarrow {}^5I_8$ transition due to partial overlap between absorption and fluorescence spectra [41]. The more serious the fluorescence trapping is, the larger the extent of spectral broadening becomes. In order to evaluate the effect of fluorescence trapping on 2 μm emission bandwidth, emission cross sections calculated from absorption and emission spectra are determined and compared. The emission cross section has been normalized to present the discrepancy of emission bandwidths, clearly.

According to the absorption spectra, the absorption cross section (σ_{abs}) can be deduced by [19,42]

$$\sigma_{abs}(\lambda) = \frac{2.303 \log(I_0/I)}{Nl} \tag{3}$$

where N is the concentration of rare earth ions, l is the thickness of the samples, and $\log(I_0/I)$ is the absorptivity from absorption spectra. The emission cross section ($\sigma_{em}(\lambda)$) can be calculated from the absorption cross section by using McCumber (MC) formula [43] as follows:

$$\sigma_{em}(\lambda) = \sigma_{abs}(\lambda) \times \frac{Z_l}{Z_u} \times \exp\left[\frac{hc}{kT} \times \left(\frac{1}{\lambda_{ZL}} - \frac{1}{\lambda}\right)\right] \tag{4}$$

where Z_l and Z_u are the partition functions for the lower and the upper levels involved in the considered optical transition, respectively. T is the temperature (here is the room temperature), k is the Boltzmann constant and λ_{ZL} is the wavelength for the transition between the lower Stark sublevels of the emitting multiplets and the lower Stark sublevels of the receiving multiplets.

The inset of Fig. 4 depicts the emission cross sections derived from absorption and fluorescence spectra using MC and FL theory, respectively. It can be found that the divergence of 2 μm emission bandwidth from MC and FL theory is very small. Thus, fluorescence trapping has hardly impact on emission bandwidth in the studied sample.

The product of $\Delta\lambda_{eff} \times \sigma_{em}^{peak}$, defined as gain bandwidth, is an important parameter to evaluate the gain performances. The larger the gain bandwidth is, the better the gain property of material becomes [33]. In this work, the value of $\Delta\lambda_{eff} \times \sigma_{em}^{peak}$ is as high as 891×10^{-28} cm^3, which is larger than those of fluoride (625×10^{-28} cm^3) [33], silicate (574×10^{-28} cm^3) [33] and germanate glass (336×10^{-28} cm^3) [33], while it is comparable to that of fluorophosphate glass (825×10^{-28} cm^3) [33]. Consequently, Ho^{3+}/Er^{3+} codoped germanosilicate glass along with higher gain bandwidth would be a suitable candidate for 2 μm laser or amplifier.

4. Discussions

In view of excellent 2.0 μm fluorescence properties of the prepared glasses, it is necessary to further investigate luminescent mechanism to optimize material design. Therefore, fluorescence spectra at 1.53 μm and 2.7 μm together with decay curves of 975 nm and 1.53 μm pumped at 808 nm were measured and energy transfer mechanism was analyzed based on measured data.

4.1. Fluorescence spectra and lifetime analysis

Fig. 5 displays the fluorescence spectra at 1.53 μm and 2.7 μm along with decay curves at 975 nm and 1.53 μm pumped at 808 nm. In Fig. 5(a), we can see Ho^{3+} concentration has little influence on the lifetime in Er^{3+}:$^4I_{11/2}$ level excluding the energy transfer from Er^{3+}: $^4I_{11/2}$ to Ho^{3+}. However, the 1.53 μm emission intensity and decay lifetime decrease with increasing Ho^{3+} concentration as shown in Fig. 5(b) and (c), indicating the existence of energy transfer from Er^{3+}: $^4I_{13/2}$ to Ho^{3+}. From Fig. 5(d), we can find the emission signals at 2.7 μm are weak. This is due to the existence of Si–O bond in present glass composition, which has the high phonon energy of ~1400 cm^{-1} [39,40]. This leads to high multiphonon relaxation probability between $^4I_{11/2}$ and $^4I_{13/2}$ levels, which consequently weakens the 2.7 μm emissions.

4.2. Energy transfer mechanism and microscopic parameters

The energy level diagrams of Ho^{3+} and Er^{3+} and energy transfer mechanism from Er^{3+} to Ho^{3+} are depicted in Fig. 6.

When the prepared sample is pumped by 808 nm LD, the electrons in Er^{3+}:$^4I_{15/2}$ ground states are populated to the higher $^4I_{9/2}$ level by ground state absorption (GSA: Er^{3+}: $^4I_{15/2}$ + 808 nm → $^4I_{9/2}$). Due to small energy gap between $^4I_{9/2}$ and $^4I_{11/2}$ level, ions in $^4I_{9/2}$ level can decay nonradiatively to the next $^4I_{11/2}$ level by multiphonon relaxation process. Then, populations in $^4I_{11/2}$ level may undergo the following processes: (1) energy transfer from Er^{3+}: $^4I_{11/2}$ to nearby Ho^{3+}: $^5I_6$ level (ET1: Er^{3+}: $^4I_{11/2}$ + Ho^{3+}: $^5I_8$ → Er^{3+}: $^4I_{15/2}$ + Ho^{3+}: $^5I_6$). Subsequently, the populations in Ho^{3+}:$^5I_6$ level can relax radiatively or nonradiatively to the next $^5I_7$ level. Finally, 2 μm emission takes place due to radiative transition to the ground state from Ho^{3+}:$^5I_7$ level (Ho^{3+}: $^5I_7 \rightarrow {}^5I_8$ + 2 μm); (2) radiative relaxation to the ground state and the Er^{3+}: $^4I_{13/2}$ level, respectively, giving rise to corresponding 975 nm and 2.7 μm radiations. On the other hand, part of ions in Er^{3+}: $^4I_{13/2}$ level can transfer their energy to adjacent Ho^{3+}: $^5I_7$ level by ET2 process (Er^{3+}: $^4I_{13/2}$ + Ho^{3+}: $^5I_8$ → Er^{3+}: $^4I_{15/2}$ + Ho^{3+}: $^5I_7$) and subsequently, the populations

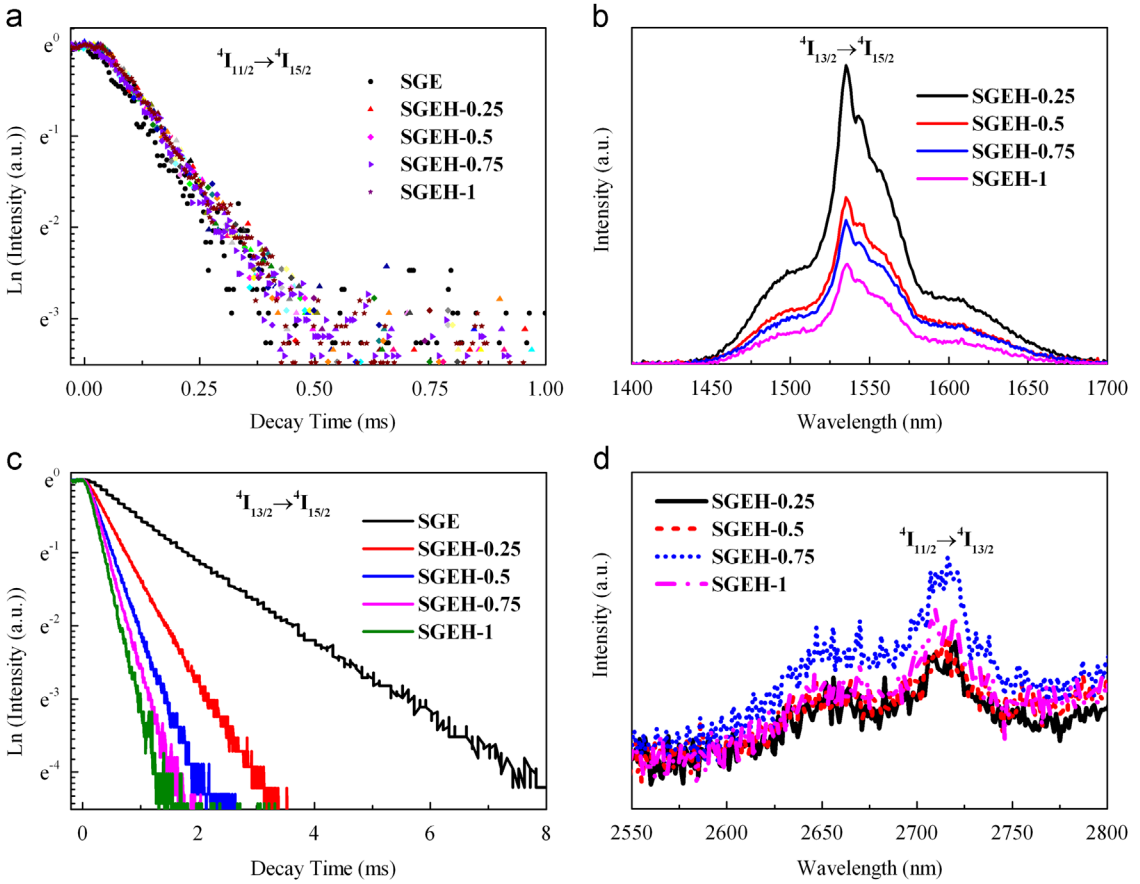

Fig. 5. (a) Decay curves at 975 nm; (b) 1.53 μm emission spectra; (c) decay curves at 1.53 μm; (d) 2.7 μm emission spectra in Er^{3+}/Ho^{3+} codoped germanosilicate glasses.

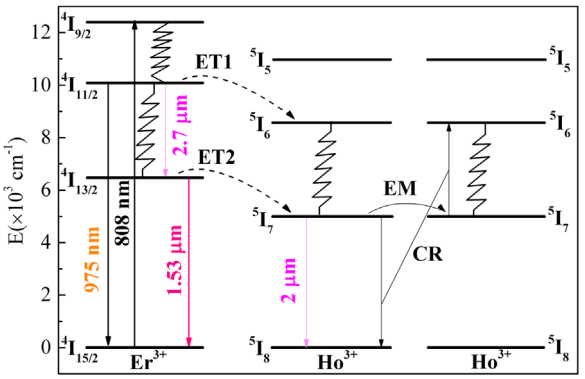

Fig. 6. Energy level diagram and energy transfer mechanism between Er^{3+} and Ho^{3+} ions in germanosilicate glass.

in Ho^{3+}: $^5I_7$ level decay radiatively to the ground state and 2 μm emission happens. In parallel, some populations in Er^{3+}: $^4I_{13/2}$ level may decay radiatively to the ground state and 1.53 μm fluorescence occur (Er^{3+}: $^4I_{13/2}\rightarrow{}^4I_{15/2}+1.53$ μm).

According to discussions mentioned above, we can summarize that both ET1 and ET2 processes can generate 2 μm fluorescence. However, from Fig. 5(a), it is found that the lifetime in Er^{3+}: $^4I_{11/2}$ level has no substantial change with increasing Ho^{3+} concentration while the 1.53 μm emission intensity and lifetimes in $^4I_{13/2}$ level decrease quickly as displayed in Fig. 5(b) and (c). It can be concluded that ET2 process is much more efficient than ET1. Hence, 2 μm emission is mainly ascribed to ET2 process. Furthermore, it is noted that 2 μm emission can be quenched when Ho^{3+} concentration is more than optimal value as revealed in Fig. 2. This phenomenon may be attributed to the energy emigration (EM: Ho^{3+}: $^5I_7\rightarrow{}^5I_7$) and cross relaxation (CR: Ho^{3+}: $^5I_7+{}^5I_7\rightarrow{}^5I_6+{}^5I_8$) processes.

In order to estimate the energy transfer (ET2) efficiency and rate from Er^{3+}: $^4I_{13/2}$ to Ho^{3+}: $^5I_7$ level, the ion lifetimes in Er^{3+}: $^4I_{13/2}$ level with and without Ho^{3+} ions have been determined from Fig. 5(c). The energy transfer rate (W_{ET}) and energy transfer efficiency (η_{ET}) were evaluated by using the following equation [38,44–46]:

$$W_{ET}=\frac{1}{\tau}-\frac{1}{\tau_0} \tag{5}$$

$$\eta_{ET}=1-\frac{\tau}{\tau_0} \tag{6}$$

where τ, τ_0 are lifetime of donor, Er^{3+} ions in the presence and absence of acceptor, Ho^{3+} ions. The derived maximum energy transfer rate is found to be 2498 s^{-1} as well as the energy transfer efficiency (η_{ET}) of 80.9%. The higher η_{ET},

compared with fluorotellurite glasses (67.33%) [47] and fluoride glass (45%) [48], is beneficial for the design of 2 μm laser under readily available high power, compact diode laser pumping.

In order to further investigate energy transfer processes between Er^{3+} and Ho^{3+} ions quantitatively, energy transfer microscopic parameters were calculated by the determination of their absorption and emission cross sections. For the dipole–dipole interaction, when phonon-assistance is taken into account, the energy transfer coefficient (C_{DA}) can be determined by the following equation [49]:

$$C_{DA}=\frac{6cg_{low}^{D}}{(2\pi)^4 n^2 g_{up}^{D}}\sum_{m=0}^{\infty} e^{-(2\bar{n}+1)S_0}\frac{S_0^m}{m!}\left(\bar{n}+1\right)^m\int \sigma_{ems}^{D}(\lambda_m^{+})\sigma_{abs}^{A}(\lambda)d\lambda \tag{7}$$

where c is the light speed in vacuum, n is the refractive index, g_{low}^{D} and g_{up}^{D} is the degeneracy of the lower and upper levels of the donor, respectively. $\hbar\omega_0$ is the maximum phonon energy, $\bar{n}=1/(e^{\hbar\omega_0/kT}-1)$ is the average occupancy of the phonon mode at T. m is the amount of phonon participating in the energy transfer. S_0 is Huang–Rhys factor and $\lambda_m^{+}=1/(1/\lambda-m\hbar\omega_0)$ is the wavelength with m phonon creation.

The absorption and emission cross sections of Er^{3+} and Ho^{3+} ions were calculated to estimate the energy transfer coefficient and are illustrated in Fig. 7. It can be observed that absorption cross section of Ho^{3+} do not overlap with emission cross section of Er^{3+}. Hence, phonons are required to assist energy transfer from Er^{3+} and Ho^{3+} ions.

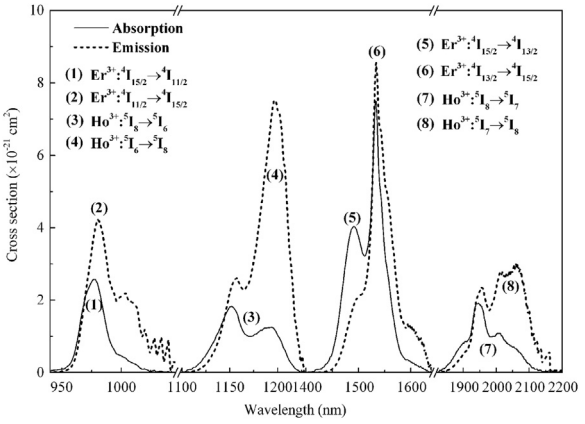

Fig. 7. Absorption and emission cross sections of Er^{3+} and Ho^{3+} in germanosilicate glass.

Table 4 tabulated the energy transfer microscopic parameters and the number of phonons necessary to assist the energy transfer process in Er^{3+}/Ho^{3+} codoped germanosilicate glasses. It can be found that the energy transfer microscopic parameter of ET2 process is as high as 4.16×10^{-40} $cm^6\,s^{-1}$, which is significantly larger than that of ET1 process (0.76×10^{-40} $cm^6\,s^{-1}$) in the prepared sample. It is proofed that ET2 process is more efficient than ET1 process. Moreover, the energy transfer of Er^{3+}:$^4I_{13/2}\rightarrow$ Ho^{3+}:$^5I_7$ is a phonon assisted nonresonant process, having the participation of zero (6.60%), one (92.64%) and two (0.76%) phonons. However, hardly no phonons assistance for Er^{3+}:$^4I_{13/2}\rightarrow Er^{3+}$:$^4I_{13/2}$ and Ho^{3+}:$^5I_7\rightarrow Ho^{3+}$:$^5I_7$ processes and the energy transfer microscopic parameter can reach 88.39×10^{-40} $cm^6\,s^{-1}$ and 13.87×10^{-40} $cm^6\,s^{-1}$, respectively. The higher microscopic parameters are due to the higher overlap between absorption and emission cross sections of Er^{3+} and Ho^{3+} ions as indicated in Fig. 7.

4.3. Rate equation analysis

To elucidate the 2 μm fluorescence behaviors with increasing Ho^{3+} concentration, a rate equation model between Er^{3+} and Ho^{3+} ions was developed according to energy level diagram of Fig. 6. Because of much lower energy transfer probability of ET1, only ET2 process is considered. Considering Er^{3+}: $^4I_{15/2}$, $^4I_{13/2}$, $^4I_{11/2}$, $^4I_{9/2}$, and Ho^{3+}: $^5I_8$ levels, the rate equations can be built as follows:

$$\frac{dn_1}{dt}=-Rn_1+A_{41}n_4+A_{31}n_3+A_{21}n_2+C_{ET}n_2n_{Ho} \tag{8}$$

$$\frac{dn_2}{dt}=A_{42}n_4+A_{32}n_3-A_{21}n_2-C_{ET}n_2n_{Ho} \tag{9}$$

$$\frac{dn_3}{dt}=A_{43}n_4-A_{31}n_3-A_{32}n_3 \tag{10}$$

$$\frac{dn_4}{dt}=Rn_1-A_{41}n_4-A_{42}n_4+A_{43}n_4 \tag{11}$$

$$n_1+n_2+n_3+n_4=n_{Er} \tag{12}$$

where n_1, n_2, n_3, n_4, n_{Er} and n_{Ho} are the population numbers of Er^{3+}: $^4I_{15/2}$, $^4I_{13/2}$, $^4I_{11/2}$, $^4I_{9/2}$, total Er^{3+} and Ho^{3+}: $^5I_8$ levels, respectively. R is the pumping rate. A_{ij} is the total transition rates from i to j level involving radiative and multiphonon relaxation contributions. C_{ET} is energy transfer rate from Er^{3+}:$^4I_{13/2}$ to Ho^{3+}:$^5I_7$ level.

Due to small energy gap between Er^{3+}:$^4I_{11/2}$ and $^4I_{9/2}$ levels and high Si-O bonding vibration phonons, the ions in $^4I_{9/2}$ level can decay quickly to $^4I_{11/2}$ level. Thus, the

Table 4
Calculated microscopic parameters C_{DA} and C_{DD} for $Er^{3+}\rightarrow Ho^{3+}$, $Er^{3+}\rightarrow Er^{3+}$ and $Ho^{3+}\rightarrow Ho^{3+}$ energy transfer in Er^{3+}/Ho^{3+} codoped germanosilicate glass. The number of phonons necessary to assist the energy transfer process is also revealed with their percent contributions.

Energy transfer	N (phonons-assist) (%)			C_{DA}($\times10^{-40}$ $cm^6\,s^{-1}$)	C_{DD}($\times10^{-40}$ $cm^6\,s^{-1}$)
Er^{3+}:$^4I_{13/2}\rightarrow Ho^{3+}$:$^5I_7$	0 (6.60)	1 (92.64)	2 (0.76)	4.16	
Er^{3+}:$^4I_{13/2}\rightarrow Er^{3+}$:$^4I_{13/2}$	0 (~100)	1 (~0)	2 (0)		88.39
Er^{3+}:$^4I_{11/2}\rightarrow Ho^{3+}$:$^5I_6$	0 (11.35)	1 (86.98)	2 (1.67)	0.76	
Ho^{3+}:$^5I_7\rightarrow Ho^{3+}$:$^5I_7$	0 (100)				13.87

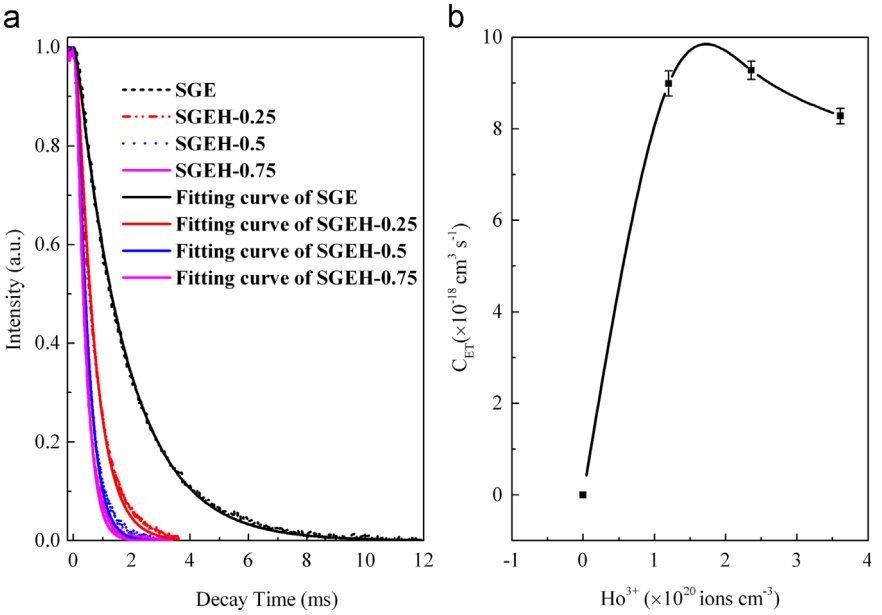

Fig. 8. (a) Measured decay data of Er^{3+}:$^4I_{13/2}$ level and best fitting curves via rate equation in germanosilicate glass; (b) calculated energy transfer rates derived from rate equation model and decay data.

equations mentioned above can be further simplified as

$$\frac{dn_1}{dt} = -Rn_1 + A_{31}n_3 + A_{21}n_2 + C_{ET}n_2n_{Ho} \tag{13}$$

$$\frac{dn_2}{dt} = A_{32}n_3 - A_{21}n_2 - C_{ET}n_2n_{Ho} \tag{14}$$

$$\frac{dn_3}{dt} = Rn_1 - A_{31}n_3 - A_{32}n_3 \tag{15}$$

$$n_1 + n_2 + n_3 = n_{Er} \tag{16}$$

By solving Eq. (15) when pumping source is switched off, the following expression can be obtained:

$$n_3(t) = n_3(0)\exp[-(A_{31}+A_{32})t] \tag{17}$$

Combining with Eqs. (14) and (17), $n_2(t)$ can be expressed as

$$\frac{n_2(t)}{n_2(0)} = \frac{A_{32}n_3(0)}{n_2(0)[A_{21}+C_{ET}n_{Ho}-A_{31}-A_{32}]}\exp[-(A_{31}+A_{32})t] + \left[1-\frac{A_{32}n_3(0)}{n_2(0)[A_{21}+C_{ET}n_{Ho}-A_{31}-A_{32}]}\right]\exp[-(A_{21}+C_{ET}n_{Ho})t] \tag{18}$$

where $n_2(0)$ and $n_3(0)$ is the excited population numbers in Er^{3+}:$^4I_{13/2}$ and $^4I_{11/2}$ level, respectively, after the pump source turns off (t=0). By solving Eq. (14) in the steady state condition ($dn_2(t)/dt$=0), the ratio of $n_3(0)$ and $n_2(0)$ can be derived as

$$\frac{n_3(0)}{n_2(0)} = \frac{A_{21}+C_{ET}n_{Ho}}{A_{32}} \tag{19}$$

According to Eqs. (18) and (19), the fitting functions of Er^{3+}:$^4I_{13/2}$ level can be determined as

$$\frac{n_2(t)}{n_2(0)} = \frac{A_{21}+C_{ET}n_{Ho}}{[A_{21}+C_{ET}n_{Ho}-A_{31}-A_{32}]}\exp[-(A_{31}+A_{32})t] - \frac{A_{31}+A_{32}}{[A_{21}+C_{ET}n_{Ho}-A_{31}-A_{32}]}\exp[-(A_{21}+C_{ET}n_{Ho})t] \tag{20}$$

Fig. 8(a) shows the decay data of Er^{3+}:$^4I_{13/2}$ level and best fitting curves via Eq. (20) in germanosilicate glass. It can be found that the measured date can be well fitted by Eq. (20). The fitted energy transfer rates C_{ET} have been plotted in Fig. 8(b). It is indicated that the energy transfer rate increases firstly and then decreases with Ho^{3+} concentration. The higher C_{ET} is beneficial for population accumulation of Ho^{3+}:$^5I_7$ level and improving corresponding 2 μm emissions. This tendency is in good agreement with the results of Fig. 2.

5. Conclusions

In summary, Er^{3+}/Ho^{3+} codoped germanosilicate glasses were prepared. Absorption and 2 μm fluorescence spectra were studied. *J–O* intensity parameters and radiative properties of Ho^{3+} ions were calculated based on Judd–Ofelt theory. Intense 2 μm emission was achieved with optimal Ho_2O_3 concentration of 0.5 mol%. Moreover, the spectral components of the 2 μm fluorescence band were analyzed and an equivalent model of four-level system was proposed to describe the 2 μm fluorescence. The prepared glass possesses high emission cross section (5.18×10^{-21} cm^2), wide effective emission bandwidth (172 nm) and large gain bandwidth (891×10^{-28} cm^3) for Ho^{3+}:$^5I_7\rightarrow{}^5I_8$ transition. In addition, to unravel 2 μm fluorescence behaviors, the energy transfer mechanism was proposed. The lifetime of Er^{3+}:$^4I_{13/2}$ and $^4I_{11/2}$ levels, 2.7 and 1.53 μm fluorescence were measured to illustrate energy transfer processes. Energy transfer efficiency (80.9%) and microscopic parameter (ET2: 4.16×10^{-40} cm^6 s^{-1}) were calculated to estimate the efficiency of 2 μm emissions.

Furthermore, a rate equation model was developed to elucidate the observed 2 μm fluorescence behaviors with Ho^{3+} concentration, numerically. Results show that Er^{3+}/Ho^{3+} codoped germanosilicate glass has potential application for 2 μm laser and amplifier.

Acknowledgment

The authors are thankful to Natural Science Foundation of Zhejiang Province (Nos. LY13F050003, LR14E020003, LY14B010004 and Q13F050009), National Natural Science Foundation of China (Nos. 61308090, 61405182, 51372235, 51172252, and 51272243), overseas students preferred funding of activities of science and technology project and International S&T Cooperation Program of China 2013DFE63070.

References

[1] Yuan J, Shen SX, Chen DD, Qian Q, Peng MY, Zhang QY. Efficient 2.0 μm emission in Nd^{3+}/Ho^{3+} co-doped tungsten tellurite glasses for a diode-pump 2.0 μm laser. J Appl Phys 2013;113:173507.
[2] Li S, Wang P, Xia H, Peng J, Lei Tang, Zhang Y, et al. Tm^{3+} and Nd^{3+} singly doped $LiYF_4$ single crystals with 3–5 um mid-infrared luminescence. Chin Opt Lett 2014;12:021601–4.
[3] Hemming A, Jackson SD, Sabella A, Bennetts S, Lancaster DG. High power, narrow bandwidth and broadly tunable Tm^{3+}, Ho^{3+}-co-doped aluminosilicate glass fibre laser. Electron Lett 2010;46:1617–8.
[4] Geng J, Wang Q, Luo T, Jiang S, Amzajerdian F. Single-frequency narrow-linewidth Tm-doped fiber laser using silicate glass fiber. Opt Lett 2009;34:3493–5.
[5] Li Z, Alam SU, Jung Y, Heidt AM, Richardson DJ. All-fiber, ultra-wideband tunable laser at 2 μm. Opt Lett 2013;38:4739–42.
[6] Geng J, Wang Q, Luo T, Case B, Jiang S, Amzajerdian F, et al. Single-frequency gain-switched Ho-doped fiber laser. Opt Lett 2012;37:3795–7.
[7] Xu R, Pan J, Hu L, Zhang J. 2.0 μm emission properties and energy transfer processes of Yb^{3+}/Ho^{3+} codoped germanate glass. J Appl Phys 2010;108:043522.
[8] Peng YP, Guo Y, Zhang J, Zhang L. Ho^{3+}/Yb^{3+}-codoped germanate-tellurite glasses for 2.0 μm emission performance. Appl Opt 2014;53:1564–9.
[9] Li M, Liu X, Guo Y, Hu L, Zhang J. Energy transfer characteristics of silicate glass doped with Er^{3+}, Tm^{3+}, and Ho^{3+} for ~2 μm emission. J Appl Phys 2013;114:243501.
[10] Li X, Zhang W. The microscopic interaction parameters for Er^{3+}/Ho^{3+} energy transfer in tellurite glasses. Physica B 2008;403:2714–8.
[11] Zhou X, Wang Y, Zhao X, Li L, Wang Z, Li Q, et al. Near-infrared quantum cutting via downconversion energy transfers in Ho^{3+}/Yb^{3+} codoped tellurite glass ceramics. J Am Ceram Soc 2014;97:179–84.
[12] Wang M, Yu C, He D, Feng S, Li S, Zhang L, et al. Enhanced 2 μm emission of Yb–Ho doped fluorophosphates glass. J Non-Cryst Solids 2011;357:2447–9.
[13] Xu R, Tian Y, Hu L, Zhang J. Efficient ~2 μm emission and energy transfer mechanism of Ho^{3+} doped barium gallium germanate glass sensitized by Tm^{3+} ions. Appl Phys B 2012;108:597–602.
[14] Li K, Zhang G, Wang X, Hu L, Kuan P, Chen D, et al. Tm^{3+} and Tm^{3+}-Ho^{3+}co-doped tungsten tellurite glass single mode fiber laser. Opt Express 2012;20:10115–21.
[15] Zhang Q, Ding J, Shen Y, Zhang G, Lin G, Qiu J, et al. Infrared emission properties and energy transfer between Tm^{3+} and Ho^{3+} in lanthanum aluminum germanate glasses. J Opt Soc Am B Opt Phys 2010;27:975–80.
[16] Yuan J, Shen SX, Wang WC, Peng MY, Zhang QY, Jiang ZH. Enhanced 2.0 μm emission from Ho^{3+} bridged by Yb^{3+} in $Nd^{3+}/Yb^{3+}/Ho^{3+}$ triply doped tungsten tellurite glasses for a diode-pump 2.0 μm laser. J Appl Phys 2013;114:133506.
[17] Kumarsingh A, Rai S, Rai A. Optical properties and upconversion in Er^{3+} and Ho^{3+} doped in lithium tellurite glass. Prog Cryst Growth Charact Mater 2006;52:99–106.
[18] Tian Y, Xu R, Zhang L, Hu L, Zhang J. Enhanced effect of Ce^{3+} ions on 2 μm emission and energy transfer properties in Yb^{3+}/Ho^{3+} doped fluorophosphate glasses. J Appl Phys 2011;109:083535.
[19] Li K, Wang G, Zhang J, Hu L. Broadband~2 μmemission in Tm^{3+}/Ho^{3+} co-doped TeO_2–WO_3–La_2O_3 glass. Solid State Commun 2010;150:1915–8.
[20] Xu R, Tian Y, Hu L, Zhang J. 2 μm spectroscopic investigation of Tm^{3+}-doped tellurite glass fiber. J Non-Cryst Solids 2011;357:2489–93.
[21] Xu RR, Wang M, Tian Y, Hu LL, Zhang JJ. 2.05 μm emission properties and energy transfer mechanism of germanate glass doped with Ho^{3+}, Tm^{3+}, and Er^{3+}. J Appl Phys 2011;109:053503.
[22] Lin H, Zhang YY, Pun EY. Fluorescence investigation of Ho^{3+} in Yb^{3+} sensitized mixed-alkali bismuth gallate glasses. Spectrochim Acta Part A 2008;71:1547–50.
[23] Wang M, Yi L, Wang G, Hu L, Zhang J. Emission performance in Ho^{3+} doped fluorophosphate glasses sensitized with Er^{3+} and Tm^{3+} under 800 nm excitation. Solid State Commun 2009;149:1216–20.
[24] Gao G, Hu L, Fan H, Wang G, Li K, Feng S, et al. Investigation of 2.0 μm emission in Tm^{3+} and Ho^{3+} co-doped TeO_2–ZnO–Bi_2O_3 glasses. Opt Mater 2009;32:402–5.
[25] Gao G, Wang G, Yu C, Zhang J, Hu L. Investigation of 2.0 μm emission in Tm^{3+} and Ho^{3+} co-doped oxyfluoride tellurite glass. J Lumin 2009;129:1042–7.
[26] Wei T, Chen F, Tian Y, Xu S. Broadband 1.53 μm emission property in Er^{3+} doped germa-silicate glass for potential optical amplifier. Opt Commun 2014;315:199–203.
[27] Wei T, Chen F, Tian Y, Xu S. Broadband near-infrared emission property in Er^{3+}/Ce^{3+} co-doped silica–germanate glass for fiber amplifier. Spectrochim Acta Part A 2014;126:53–8.
[28] Judd B. Optical absorption intensities of rare-earth ions. Phys Rev 1962;127:750–61.
[29] Ofelt GS. Intensities of crystal spectra of rare-earth ions. J Chem Phys 1962;37:511–20.
[30] Xu R, Tian Y, Hu L, Zhang J. Origin of 2.7 μm luminescence and energy transfer process of Er^{3+}: $^4I_{11/2}\rightarrow{}^4I_{13/2}$ transition in Er^{3+}/Yb^{3+} doped germanate glasses. J Appl Phys 2012;111:033524.
[31] Babu P, Seo HJ, Kesavulu CR, Jang YH, Jayasankar CK. Thermal and optical properties of Er^{3+}-doped oxyfluorotellurite glasses. J Lumin 2009;129:444–8.
[32] Nachimuthu P, Jagannathan R. Judd–Ofelt parameters, hypersensitivity, and emission characteristics of Ln^{3+} (Nd^{3+}, Ho^{3+}, and Er^{3+}) ions doped in PbO–PbF_2 glasses. J Am Ceram Soc 1999;82:387–92.
[33] Yi LX, Wang M, Feng SY, Chen YK, Wang GN, Hu LL, et al. Emissions properties of Ho^{3+}: $^5I_7\rightarrow{}^5I_8$ transition sensitized by Er^{3+} and Yb^{3+} in fluorophosphate glasses. Opt Mater 2009;31:1586–90.
[34] Tao L, Tsang YH, Zhou B, Richards B, Jha A. Enhanced 2.0 μm emission and energy transfer in $Yb^{3+}/Ho^{3+}/Ce^{3+}$ triply doped tellurite glass. J Non-Cryst Solids 2012;358:1644–8.
[35] Li X, Liu X, Zhang L, Hu L, Zhang J. Emission enhancement in Er^{3+}/Pr^{3+}-codoped germanate glasses and their use as a 2.7 μm laser material. Chin Opt Lett 2013;11:121601–3.
[36] Tian Y, Xu R, Hu L, Zhang J. 2.7 μm fluorescence radiative dynamics and energy transfer between Er^{3+} and Tm^{3+} ions in fluoride glass under 800 nm and 980 nm excitation. J Quant Spectrosc Radiat Transf 2012;113:87–95.
[37] Payne SA, Chase L, Smith LK, Kway WL, Krupke WF. Infrared cross-section measurements for crystals doped with Er^{3+}, Tm^{3+}, and Ho^{3+}. IEEE J Quantum Electron 1992;28:2619–30.
[38] Balaji S, Sontakke AD, Sen R, Kalyandurg A. Efficient ~2.0 μm emission from Ho^{3+} doped tellurite glass sensitized by Yb^{3+} ions: Judd–Ofelt analysis and energy transfer mechanism. Opt Mater Express 2011;1:138–50.
[39] Majérus O, Cormier L, Neuville DR, Galoisy L, Calas G. The structure of SiO_2–GeO_2 glasses: a spectroscopic study. J Non-Cryst Solids 2008;354:2004–9.
[40] Santos LF, Wondraczek L, Deubener J, Almeida RM. Vibrational spectroscopy study of niobium germanosilicate glasses. J Non-Cryst Solids 2007;353:1875–81.
[41] Wei T, Chen F, Tian Y, Xu S. 1.53 μm emission properties in Er^{3+} doped Y_2O_3 and Nb_2O_5 modified germanate glasses for an optical amplifier. J Lumin 2014;154:41–5.
[42] Gao G, Peng M, Wondraczek L. Temperature dependence and quantum efficiency of ultrabroad NIR photoluminescence from Ni^{2+} centers in nanocrystalline Ba–Al titanate glass ceramics. Opt Lett 2012;37:1166–8.

[43] McCumber D. Einstein relations connecting broadband emission and absorption spectra. Phys Rev 1964;136:A954–7.
[44] Gao G, Wondraczek L. Near-infrared down-conversion in Mn^{2+}–Yb^{3+} co-doped Zn_2GeO_4. J Mater Chem C 2013;1:1952–8.
[45] Gao G, Wondraczek L. Near-infrared downconversion in Pr^{3+}/Yb^{3+} co-doped boro-aluminosilicate glasses and $LaBO_3$ glass ceramics. Opt Mater Express 2013;3:633–44.
[46] Gao G, Peng M, Wondraczek L. Spectral shifting and NIR down-conversion in Bi^{3+}/Yb^{3+} co-doped Zn_2GeO_4. J Mater Chem C 2014;2:8083–8.
[47] Ma Y, Huang F, Hu L, Zhang J. Er^{3+}/Ho^{3+}-codoped fluorotellurite glasses for 2.7 μm fiber laser materials. Fibers 2013;1:11–20.
[48] Huang F, Liu X, Li W, Hu L, Chen D. Energy transfer mechanism in Er^{3+} doped fluoride glass sensitized by Tm^{3+} or Ho^{3+} for 2.7 μm emission. Chin Opt Lett 2014;12:051601.
[49] Tarelho L, Gomes L, Ranieri I. Determination of microscopic parameters for nonresonant energy-transfer processes in rare-earth-doped crystals. Phys Rev B 1997;56:14344–51.